Flow Measurement and Instrumentation 45 (2015) 247–254

Contents lists available at ScienceDirect

Flow Measurement and Instrumentation

journal homepage: www.elsevier.com/locate/flowmeasinst

The effect of low Reynolds number flows on pitot tube measurements

Ryan B. Spelay [a,*], Kofi Freeman Adane [a,1], R. Sean Sanders [c], Robert J. Sumner [b,2], Randall G. Gillies [a]

[a] Saskatchewan Research Council, Pipe Flow Technology Centre™, Saskatoon, SK, Canada
[b] Department of Chemical Engineering, University of Saskatchewan, Saskatoon, SK, Canada
[c] Department of Chemical and Materials Engineering, University of Alberta, Edmonton, AB, Canada

ARTICLE INFO

Article history:
Received 27 August 2014
Received in revised form
4 May 2015
Accepted 1 June 2015
Available online 6 June 2015

ABSTRACT

An investigation on the low Reynolds number effect on hemispherical-tipped Pitot tube measurements was performed by measuring the center-line velocity during the laminar flow of a Newtonian fluid in a 25 mm (1 in.) diameter vertical recirculating pipe loop. The primary objective of the study was to re-consider the available low Reynolds number Pitot tube data in the literature with modern instrumentation.

Using the results of this experimental study, a correlation that accurately predicts the low Reynolds number Pitot tube behavior has been developed. The correlation accounts for an additional viscous term in the relationship for the pressure coefficient (C_p) which is not accounted for in Bernoulli's Equation. The correlation is semi-empirical and accurately fits experimental data gathered in this study, as well as a significant body of experimental data available in the literature. The correlation, which is based on a Pitot tube Reynolds number calculated using the opening diameter (d), has been shown to be provide more accurate predictions of C_p for a wide range of opening diameter to outer diameter ratios ($0.22 \leq d/D \leq 0.6$) than available correlations based on outer diameter.

The transition Pitot tube Reynolds number, below which Bernoulli's Equation is no longer appropriate, was predicted to be approximately 35, compared to a value of 79 obtained from fitting data collected by Barker. The correlation developed in this study provides smoother transitions at both ends of the low Reynolds range. At the low end ($Re < 10$) it converges with a Stokes Law' analogy, while at the critical transition ($Re \sim 35$) it converges asymptotically with Bernoulli's Equation. The correlation also accurately predicts the behavior of the pressure coefficient with Reynolds numbers between these ranges.

1. Introduction

A Pitot tube is a differential pressure anemometer that allows for the measurement of a single, localized velocity component, when it is aligned streamwise to the flowing fluid. It operates on the basis that fluid kinetic energy is converted to pressure energy upon stagnation of fluid at the Pitot tube tip. Under most conditions the stagnation pressure can be related to the local velocity using Bernoulli's Equation:

$$C_p = \frac{P - P_\infty}{\frac{1}{2}\rho v_\infty^2} = 1 \quad (1)$$

Pitot tubes are an intrusive velocity measurement instrument [1]. Although they can be used to measure the local velocity of flowing fluids, numerous studies have indicated limitations at extreme Reynolds numbers (high and low), where errors can result from the use of Bernoulli's Equation to calculate the velocity. This is particularly true at low Reynolds numbers where viscous effects, not considered in Bernoulli's Equation, become important. The inability of Bernoulli's Equation to adequately capture Pitot tube behavior at low Reynolds number flows is related to two important limitations: Bernoullli's equation is applicable only along a fluid streamline and it cannot account for viscous effects, i.e. it accounts only for the conversion of kinetic energy to pressure energy. At low Reynolds numbers, the fluid streamlines turn away from the face (tip) of the Pitot tube farther upstream than at higher Reynolds numbers where $C_p \sim 1$ [2]. An excellent study of this subject was published recently by Boetcher and Sparrow [2].

The low cost of Pitot tubes relative to other velocity

* Corresponding author.
E-mail address: spelay@src.sk.ca (R.B. Spelay).
[1] Now with: Alberta Innovates Technology Futures, Edmonton, Canada.
[2] Now with: Cameco Corp., Saskatoon, Canada.

http://dx.doi.org/10.1016/j.flowmeasinst.2015.06.008
0955-5986/

Nomenclature

A	cross-sectional area of flow in the pipe (m^2)
a	low Reynolds number Pitot tube correlation parameter, (Eq. (11))
b	low Reynolds number Pitot tube correlation parameter, (Eq. (11))
C_h	specific heat capacity at constant pressure, ($J\ kg^{-1}\ K^{-1}$)
C_p	pressure coefficient (Eq. (1))
d	Pitot tube opening diameter (m)
D	Pitot tube outside diameter (m)
D_p	pipe diameter (m)
h	specific enthalpy ($J\ kg^{-1}$)
k	thermal conductivity ($W\ m^{-1}\ K^{-1}$)
NPS	Nominal Pipe Size (m)
P	pressure (Pa)
ΔP	measured pressure drop over the test section (Pa)
P_z	frictional pressure gradient over the test section ($Pa\ m^{-1}$)
P_∞	static pressure (Pa)
Q	volumetric flowrate ($m^3\ s^{-1}$)
r	radial direction in pipe, cylindrical coordinates (m)
R	inside radius of pipe (m)
Re_d	Pitot tube Reynolds number using the diameter of the Pitot opening (Eq. (3a))
Re_D	Pitot tube Reynolds number using the outside diameter of the Pitot (Eq. (3b))
Re_t	transition Reynolds number below which $C_p \neq 1$ (based on the diameter of the Pitot opening)
S	specific gravity (dimensionless)
v	local velocity ($m\ s^{-1}$)
v_∞	Local freestream fluid velocity ($m\ s^{-1}$)
T	fluid temperature (K)
V	bulk (average) mixture velocity ($m\ s^{-1}$)

Greek symbols

β	ratio of Pitot tube inside to outside diameters (d/D), (Table 1)
μ	Newtonian viscosity ($Pa \cdot s$)
ρ	Fluid density ($kg\ m^{-3}$)
τ	fluid shear stress (Pa)

Subscripts

i	inlet
w	wall

measurement techniques, and their simplicity in terms of operation and installation, means that they are commonly used in a wide variety of industrial applications. Examples include application as an averaging flow meter [3], in the flows of heavy liquid metals [4], in gas–liquid multiphase flow measurements [5–8], and extensively to measure velocity profiles in solid–liquid (slurry) pipeline flows (see Mishra et al. [9] for a good review). Most of these applications, to date, have been for high velocity flows and at lower viscosities so that Bernoulli's Equation applies and $C_p=1$ and, perhaps equally as important, is constant i.e. independent of Reynolds number. Interest in the effect of low Reynolds number flow on Pitot tube measurements relates directly to ongoing studies of the behavior of multiphase mixtures in pipes and open channels, including mixtures of heavy oil and water [10] and solids–liquid mixtures [11,12]. In addition, the results of this study are important if the gas–liquid multiphase flow Pitot tube applications mentioned earlier are extended to mixtures containing high-viscosity liquids, such as heavy crude oils.

2. Background

Barker [13] conducted pioneering research with Pitot tubes at low Reynolds numbers. She performed experimental testing with water using a bench top apparatus and a single Pitot tube. Her findings showed that a Stokes' Law analogy [14] could be used to describe the phenomenon occurring at the tip of the Pitot tube at low Reynolds numbers. However, results of more recent studies, including this investigation, have shown that this analogy is not appropriate over the entire low Reynolds number regime. The correction factor applied by Barker to account for low Reynolds number viscous effects on Pitot tube measurements is given as

$$C_p = 1 + \frac{6}{Re_d} \tag{2}$$

The Reynolds number based on the opening diameter of the Pitot tube (d) is

$$Re_d = \frac{\rho d v}{\mu} \tag{3a}$$

Alternatively, the Reynolds number can be expressed as a function of the outside diameter, D, of the Pitot tube:

$$Re_D = \frac{\rho D v}{\mu} \tag{3b}$$

A thorough review of Pitot tube performance was conducted by Folsom [15]. Even though only a small section of the paper was devoted to the low Reynolds number effect on Pitot tube performance, much of the focus was on the theoretical work of Homann [16] and Chambre [17], who developed corrections for Pitot tube measurements at low Reynolds numbers. However, their results, along with those presented by Folsom [15] and Perry [18], were correlated using the outside diameter (D) of the Pitot tube. As well, their focus was for Pitot tubes of varying tip shapes, but only limited literature was provided for the hemispherical tipped Pitot tubes used in this study.

Two important studies are those of MacMillan [19,20], where it was suggested that the opening diameter (d) of the Pitot tube appears be the more appropriate scaling parameter. The scatter in experimental results reported by those using the Pitot tube outside diameter as the correlating parameter was reduced when the data were reanalyzed using the opening diameter of the Pitot tube.

Mikhailova and Repik [21,22] made measurements with Pitot tubes having varying inside-to-outside diameter ratios. They showed that both the choice of length scale and the ratio of the inside to outside diameters of the Pitot tube are important parameters for Pitot tube calculations. For thin-walled Pitot tubes ($d/D \sim 1$), they found no difference in results when either the inside or the outside diameter was used as a length scale. However, as the ratio of the two diameters decreases (thick walled Pitot tubes, hemispherical Pitot-static tubes), they found that the inside diameter was the more appropriate scaling parameter.

Hurd et al. [23] performed experiments with blunt nose impact tubes in a tow tank with viscous incompressible liquids. No

correlation resulted from the study but they showed that for high d/D ratios the value of C_p can drop below 1 at intermediate Re numbers. It was also shown that at very low Reynolds numbers their Pitot tube results asymptotically converged to Stokes' Law [23]. They pointed out that the correlations developed by Homann [16] and Chambre [17] do not converge with Stokes' Law at very low Reynolds numbers.

From the references described here, it can be seen that most of the research on low Reynolds number Pitot tube effects was conducted in the 1950s. More recently, a study was conducted by Chebbi and Tavoularis [24], who used laser Doppler anemometry to experimentally verify Pitot tube measurements at very low Reynolds numbers ($Re_d \ll 1$). However, due to the complexity of the experimental technique, only a limited number of measurements were performed. Although this was an important study in terms of validating Pitot tube measurements, it is not applicable to measurements made in the operating range $1 < Re_d < 100$.

Boetcher and Sparrow [2] also conducted numerical simulations to study the low Reynolds number Pitot tube behavior. Their results showed that the transition Reynolds number, where Bernoulli's Equation can no longer be applied, was dependent on the Pitot tube tip shape for a diameter ratio of $d/D = 0.31$. Hemispherical shaped tubes were shown to transition at lower Reynolds numbers than flat-nosed tubes.

3. Experimental method

3.1. Equipment

Tests were conducted at the SRC Pipe Flow Technology Centre™ with two sizes of hemispherical tipped Pitot-static tubes. A significant quantity of low Reynolds number data was generated by performing experiments using a 25 mm NPS vertical recirculating pipe loop employing ethylene glycol over a wide range of flow conditions. A schematic of the SRC 25 mm NPS vertical pipe loop is shown in Fig. 1.

The pipe loop circuit consisted of a conical-bottom stand tank, a progressive cavity pump, a vertical run of 27.67 mm inside diameter carbon steel pipe on the downflow side, and a 25.80 mm inside diameter vertical run of stainless steel pipe on the upflow side. In total, the apparatus spanned a height of 8.68 m and held 17.53 L of fluid (not including the supply tank).

A progressive cavity pump was used to produce flow within the pipe system. A 15 kW (20 hP) motor was used to drive the pump. The rotational speed of the motor was controlled by a variable frequency drive (VFD). The temperature of the fluid in the circuit was measured with a temperature sensor located directly following the pump outlet. A chilled ethylene glycol–water mixture was circulated through the heat exchangers to maintain isothermal conditions in the system ($\pm$ 0.5 °C). One co-current (3.75 m) and one counter-current (3.90 m) pipe-over-pipe heat exchanger were employed on the downflow and upflow sections, respectively.

The Pitot tube assembly was located 241 pipe diameters (6.1 m) downstream from the temperature sensor in the downflow section of the loop. The Pitot tube was positioned at the center of the pipe where it was locked into position. The pressure difference between the stagnation and static pressure seen by the Pitot tube was measured with a differential pressure transducer with a 5 psi (34.5 kPa) diaphragm. It should be noted that although a 5 psi diaphragm was installed to minimize the likelihood of diaphragm damage from transient events such as pump speed changes, it was calibrated for operation in the 0–2 psi (0–14 kPa) range. The pressure transducer was calibrated against a manometer containing Meriam fluid ($S = 2.95$).

Two hemispherical tipped Pitot-static tubes (United Sensor Corporation) were employed in the study. The larger Pitot tube was referred to as 'PSL' (Pitot-Static Large), while the smaller Pitot tube was referred to as 'PSS' (Pitot-Static Small). The outside diameters of the Pitot tubes, D, were measured using digital calipers. The accuracy of the calipers was of the order of 0.01 mm. The outside diameter of each Pitot tube was determined from the average of five measurements. The inside diameter of the Pitot tube opening, d, was determined using a digital camera. Four digital photographs of the tip of each Pitot tube were analyzed to determine the inside diameter of the opening. The Pitot tube dimensions are presented in Table 1. Fig. 2 illustrates the geometry of a hemispherical-tipped Pitot tube.

A Foxboro magnetic-flux flowmeter was located directly downstream of the Pitot assembly and was used to measure the volumetric flowrate in the system, from which the average flow velocity V could be directly calculated. The flow meter was calibrated to ensure it provided accurate readings for the flow of

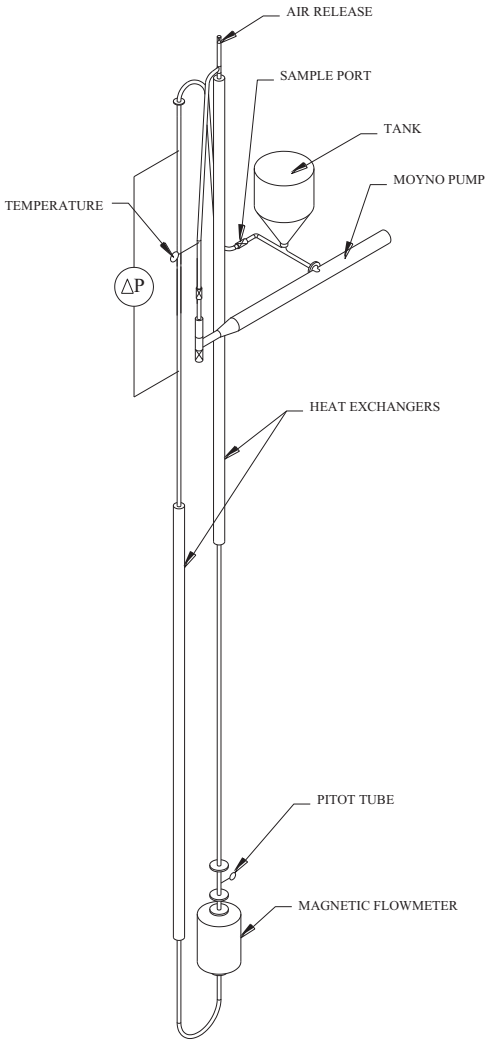

Fig. 1. Schematic illustration of the SRC 25 mm diameter vertical pipe loop.

Table 1
Dimensions of Pitot-static tubes.

	PSL Mean	Std. Dev	PSS Mean	Std. Dev
D (mm)	3.06	0.01	1.62	0.01
d (mm)	1.13	0.02	0.52	0.03
β (d/D)	0.37	0.01	0.32	0.02

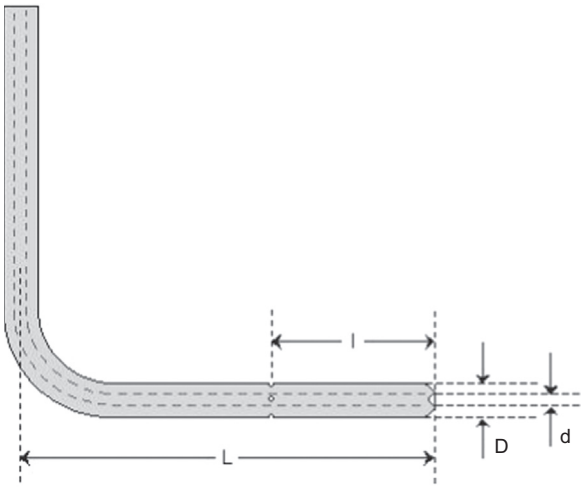

Fig. 2. Schematic illustration of the geometry of the Pitot tubes used in the present study.

glycol under laminar flow conditions. Flow meter performance was validated against the Moyno pump flow curve, because the pump, under the conditions tested, acts as a positive displacement pump.

The pressure drop (ΔP) was measured using a differential pressure transducer, with a 20 psi (138 kPa) diaphragm, that was calibrated against a Meriam fluid (S=2.95) manometer. The test section was 1.83 m in length and the upstream pressure tap was located approximately 216 pipe diameters (5.6 m) from the 180° elbow, which ensured fully developed flow in the test section. By measuring the pressure drop and subtracting the pressure change due to the elevation change over the test section, the frictional pressure gradient was obtained. The frictional pressure gradient, P_z, was used to determine the on-line (real time) viscosity of the fluid, as described in the following section.

The instruments were connected to an InstruNet® data board and a DasyLab® data acquisition system. Each of the instruments produced either a 0–5 V or a 4–20 mA signal. The instruments were calibrated over the desired ranges so that they produced measurements with the optimum resolution. The signals produced by the instruments were conditioned with the DasyLab software and collected directly to a Microsoft Excel® spreadsheet on a personal desktop computer using Visual Basic® macros.

A full, detailed description of the apparatus is provided elsewhere [25].

3.2. Materials

Automotive grade ethylene glycol (NemCo Resources Ltd.) was used as the process (test) fluid, for three main reasons: it is a Newtonian fluid, it allowed for operation in the range of interest, i.e. $Re_d < 100$, and its variation in density and viscosity with temperature are easily characterized. With respect to the last point, the variation of density with temperature was measured in the laboratory using a pycnometer to obtain the following correlation:

$$\rho = 1137.2 - 0.699(T - 273.15) \tag{4}$$

where ρ is the glycol density and has units of kg/m^3 and T is temperature in Kelvin.

The pressure measurement test section in the upflow section of the pipe loop was used to determine the Newtonian viscosity (μ) of the ethylene glycol in laminar flow. Specifically, the Hagen–Poiseuille equation was used to calculate the glycol viscosity at different system temperatures from the frictional component of the pressure drop over the test section and the volumetric flow rate:

$$\mu = \frac{P_z\, \pi\, D_p{}^4}{128Q} \tag{5}$$

The measurements were used to develop the following correlation for viscosity as a function of temperature:

$$\mu = \exp\left[5.006 - \frac{4917}{T} + \frac{1.275 \times 10^6}{T^2}\right] \tag{6}$$

Again, the temperature, T, is expressed in degrees Kelvin and the viscosity is given in 'mPa · s'. The accuracy of the viscosity–temperature correlation was validated by making measurements using a Haake RS-150 concentric cylinder viscometer.

3.3. Procedures

Tests were performed at low Reynolds numbers under steady, fully developed, laminar flow conditions. Under these conditions it is known that the velocity of a Newtonian fluid at the centerline of the pipe ($r=0$) is equal to twice the bulk velocity, i.e.

$$v(r) = 2V\left(1 - \frac{r^2}{R^2}\right) \tag{7}$$

This allowed the velocity at the Pitot tube to be calculated explicitly for each volumetric flowrate tested. One concern, since it was not possible to change the radial position of the Pitot tube, was the possibility that the true velocity profile might not exactly follow Eq. (7) because of the operation of the pipe-over-pipe heat exchanger upstream of the Pitot tube. Recall that chilled glycol was circulated through the annulus of this heat exchanger to sufficiently cool the process fluid so that measurements could be made at low Pitot Reynolds numbers ($Re_d < 10$). Specifically, the pipe walls within the heat exchanger would be at a temperature different from the process fluid temperature, meaning that radial variations in the density and viscosity of the glycol would occur.

In order to evaluate the extent to which the heat exchangers could cause the velocity profile to deviate from that expected for laminar, Newtonian pipe flow, a series of numerical simulations was conducted. The details of the simulations are given in the next section, while the results are discussed in Section 5.1.

4. CFD simulations

Numerical solutions were obtained using ANSYS CFX-13.0. Although a number of test cases were simulated, only four are presented here (see Table 2), as these represent the conditions where the variation between the process fluid temperature and pipe wall temperature was the greatest. In other words, the simulations described here are for the cases expected to have the greatest radial variation in fluid temperature – which would lead to the greatest error in the assumption of perfect Poiseuille flow.

Table 2
Upstream section inlet conditions for numerical simulations.

Case	V (m/s)	T_i (°C)	Re_d[a]	T_w (°C)
1	0.15	4.9	3.9	−10.0
2	0.26	5.3	6.8	−10.0
3	0.78	5.7	21	−10.0
4	0.55	15.1	24	2.0

[a] Note: values of Re_d given in the table correspond to the smallest diameter Pitot tube (PSS) tested, and are based on the fluid properties calculated using T_i.

The governing equations for steady, laminar, Newtonian flow can be written as follows:

Continuity

$$\nabla\cdot\left(\rho\,\vec{\nu}\right) = 0 \tag{8}$$

Momentum equation

$$\nabla\cdot\left(\rho\;\vec{\nu}\;x\;\vec{\nu}\right) = -\nabla P + \nabla\cdot\bar{\bar{\tau}} \tag{9a}$$

where

$$\bar{\bar{\tau}} = \mu\left(\nabla\vec{\nu} + \left(\nabla\,\vec{\nu}\right)^{t} - \tfrac{2}{3}\delta\,\nabla\cdot\vec{\nu}\right) \tag{9b}$$

Energy equation

$$\nabla\cdot\left(\rho\,h\,\vec{\nu}\right) = \nabla\cdot(k\nabla T) + \bar{\bar{\tau}}\colon\nabla\vec{\nu} \tag{10a}$$

with

$$dh = C_h\,dT + \left.\frac{\partial h}{\partial P}\right|_T dP \tag{10b}$$

In Eqs. (8)–(10), $\vec{u}$ represents the velocity vector, P is the pressure, T is the fluid temperature, t is the transpose operator function, δ is the identity matrix or Kronecker delta function, h is enthalpy, C_h is specific heat capacity at constant pressure and k is the thermal conductivity. For these simulations, constant values of C_h and k were assumed: 2.279 kJ kg^{-1} K^{-1} and 0.3041 W m^{-1} K^{-1}, respectively. The fluid density and dynamic viscosity were assumed to be a function of temperature only, and the correlations given previously (Eqs. (4) and (6)) were implemented via user-defined functions.

The flow domain was divided into two parts: upstream and downstream, and computations were done separately for the two flow domains. The output of the 'upstream' simulations represented the inlet boundary conditions for the 'downstream' simulations. This was done to reduce computational power and to simplify the analysis. The 'upstream' domain is the process piping within the heat exchanger that is upstream of the Pitot tube. The 'downstream' domain starts at the discharge of the aforementioned heat exchanger and includes the Pitot tube.

The inlet boundary conditions for the upstream section are given in Table 2 for each test case. Note that it was assumed that the inlet temperature is that measured with the temperature sensor (see Fig. 1). It was also assumed that the pipe wall temperature was equal to that of the heat exchange fluid being circulated through the annulus of the heat exchanger, i.e. the thermal resistance of the metal pipe wall was neglected.

A no-slip boundary condition was applied at the pipe wall for both the upstream and downstream sections. At the outlet of each section, a zero average pressure condition was specified. For the upstream section, it should be mentioned that a pipe length of 4.5 m was used instead of the 3.9 m for the actual problem definition. This was done to avoid any effect of the outlet boundary condition on the results at the actual length of the section (i.e. 3.9 m).

For the downstream section, the data extracted at the exit of the upstream section (3.9 m) were used as inlet boundary conditions. These data included the radial distributions of velocity, temperature (and therefore also fluid density and viscosity) and pressure. Since this flow domain is exposed to the surrounding ambient fluid, i.e. air at 20 °C, heat flux was specified at the wall using this temperature and convective heat transfer coefficient, h_o=5 W m^{-2} K^{-1}, was selected based on the properties of air at 20 °C. The numerical simulations of the downstream section were also repeated assuming an adiabatic boundary condition at the wall. As we will show in the next section, the simulation results were not sensitive to this particular boundary condition. Here again, the pipe length of 4.5 m was used for the simulations but the results at z=3.75 m (i.e. the actual distance between the discharge of the heat exchanger and the Pitot tube) were extracted from the simulations.

Mass conservation discretization on the non-staggered grid is an adaptation of earlier techniques by Rhie and Chow [26]. A standard finite element derivative approximation via shape functions is used for the diffusion terms. The high resolution scheme (HRS), which is based on the formulation of Barth and Jesperson [27], was used for advection terms. It should be mentioned that HRS is a blend of both first and second order schemes with the blending factor being a function that is computed locally.

The discretized mass and momentum conservation equations were fully coupled and solved simultaneously using additive correction multigrid to accelerate convergence. Double precision was used in the computations and solutions were considered converged when the normalized sum of the absolute dimensionless residuals of the discretized equations was less than 10^{-6}.

A five-block structured computational mesh representing the entire domain was created using ANSYS ICEMCFD and then imported into ANSYS CFX. The grid is made up of O-grids. Grid independence tests were performed and a mesh of 422,800 was sufficient for grid independence for each of the two flow domains (upstream, downstream).

5. Results and discussion

5.1. Numerical simulations

Fig. 3 shows the simulation results for the 4 different cases described in Table 2. Recall that the conditions expected to provide a velocity profile deviating most widely from the ideal Poiseuille case were simulated: specifically, cases where the flowrate was low and the difference between the wall temperature and inlet (well-mixed) fluid temperature was greatest. The difference between the centerline velocity under isothermal conditions (ν_{max}=2 V) and those expected because of the radial temperature (and therefore, fluid viscosity and density) variation was between 5.2% (Case 4) and 7.4% (Case 1). All the results reported in the following section were corrected based on the simulation results. Additionally, the results are shown with horizontal and vertical error bars of 10% based on an overall error analysis.

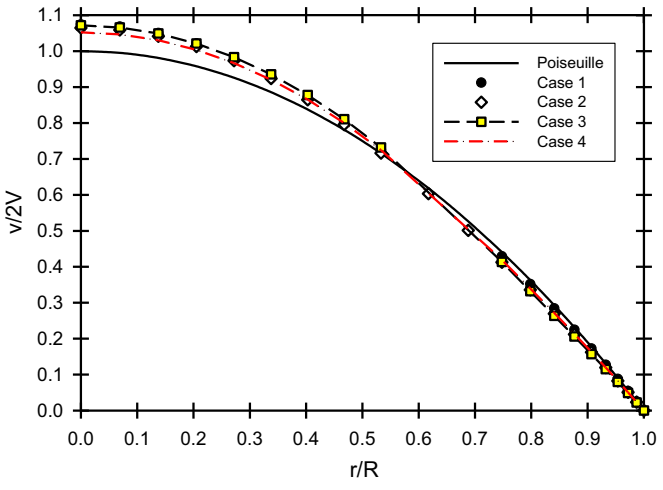

Fig. 3. Velocity profiles for ideal (isothermal) Poiseuille flow and for the 4 cases described in Table 2. Note that radial variations in temperature, fluid viscosity and density for Cases 1–4 cause the non-ideal velocity profiles.

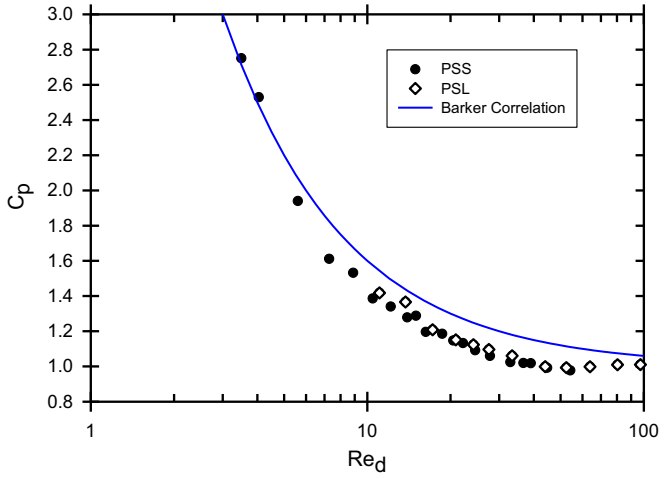

Fig. 4. Low Reynolds number Pitot tube pressure coefficient data obtained during the present study, compared with the predictions of Barker [13].

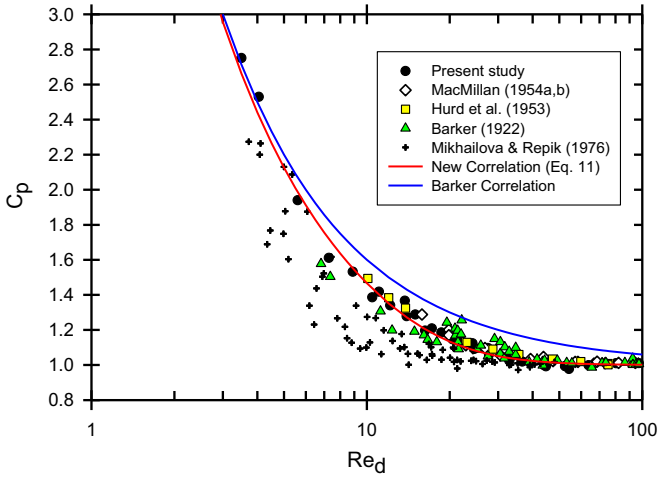

Fig. 5. Correlations and experimental data for low Reynolds number Pitot tube measurements plotted as a function of Re_d.

5.2. Low Reynolds number measurements ($Re_d < 100$)

The experimental program conducted in the present study included more than 700 low Reynolds number Pitot tube measurements. The tests were conducted over the range $3 < Re_d < 120$. Averaged data collected at each condition are shown in Fig. 4, which provides a comparison of the experimentally determined pressure coefficients obtained during the present study plotted against the Reynolds number based on the inside diameter of the Pitot tube for both Pitot tubes (PSS and PSL).

Examination of the data of Fig. 4 shows that the transition Reynolds number (Re_t, based on the opening diameter of the Pitot tube, d), where Bernoulli's Equation (i.e. $C_p=1$) is no longer appropriate, occurs at a value less than 40. Asymptotic analysis of the experimental results yields $Re_t=35$ for the experimental data set of the present study. This is in good agreement with the numerical simulation results of Boetcher and Sparrow [2]. Although they used the outer Pitot tube radius as their length scale, when their results are re-analyzed using the diameter of the tube opening, transition Reynolds numbers of 28 and 40 were predicted for hemispherical tipped and flat-nosed tubes, respectively.

The experimental low Reynolds number data of this study can be correlated by selecting only the data points where the Pitot tube Reynolds number is below the transition value ($Re=35$). The form of the equation selected for the correlation is similar to the equations used by Homann [16] and Chambre [17]:

$$C_p = 1 + \frac{6}{\mathrm{Re}_d + a\mathrm{Re}_d^b} \tag{11}$$

Values of the correlation parameters, a and b, were obtained by applying the Levenberg–Marquardt minimization method [28]. The parameter in the numerator was set to 6 so that the equation reduces to Stokes' Law (Eq. (2)) at very low Reynolds numbers ($\mathrm{Re}\to 0$). The best fit parameters for the low Reynolds number correlation based on the experimental data of the present study are $a=0.00217$ and $b=3.12$.

Previous studies (see Ref. [15]) suggest that the parameters a and b are related to the shape and specific geometry of the Pitot tube tip. As a result, this correlation is appropriate for hemispherical tipped Pitot tubes of the type used in this investigation. Specific attention should be paid to the fact that the diameter of the Pitot tube opening is used to calculate the Pitot tube Reynolds number. A review of the literature in this area, however, indicates that the choice of the Pitot opening (d) over the use of the Pitot tube outer diameter (D) requires further explanation.

Low Reynolds number Pitot data obtained by other researchers are presented in Figs. 5 and 6, along with the data obtained in the present study. Note that tests were conducted using Pitot tubes with diameter ratios from 0.22 [19] to 0.854 [21], with the measurements of the present study conducted using Pitot tubes with diameter ratios of 0.32 and 0.37 (see Table 1). Fig. 5 presents the data as a function of $\mathrm{Re_d}$. Barker's [13] correlation (Eq. (2)) and the correlation developed in the present study (Eq. (11), with $a=$ 0.00217 and $b=3.12$) are also provided on the figure. Barker's data are shown only on Fig. 5; interestingly, she did not explicitly indicate if the reported "Pitot tube diameter" referred to the tube opening (d) or outer diameter (D), although careful review of both her work [13] and the subsequent proof provided by MacMillan [19] strongly suggest Barker reported the value of 'd'. The excellent agreement between correlation developed here (Eq. (11)) and Barker's data support this conclusion. Because Fig. 6 presents the experimental pressure coefficient data plotted against the Reynolds number based on the outside diameter of the Pitot tube ($\mathrm{Re_D}$), the correlations developed by Homann [16] and Mikhailova and Repik [21] are shown alongside the experimental results.

The experimental data collected during the present study, and the correlation developed here (Eq. (11), with $a=$ 0.00217 and $b=3.12$), are in excellent agreement with the earlier experimental results [13,19,21,23] when plotted as a function of Re_d, as shown in Fig. 5. When one compares the use of $\mathrm{Re_d}$ as a correlating

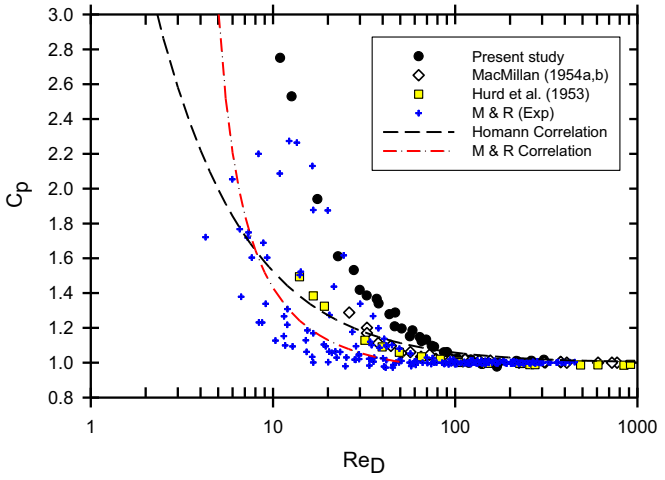

Fig. 6. Correlations and experimental data for low Reynolds number Pitot tube pressure coefficients plotted as a function of Re_D.

parameter (Fig. 5) with the use of Re_D (Fig. 6), it is evident that the data available in the literature appear to collapse more uniformly with Re_d than with Re_D. It would be naïve, however, to state a general preference for Re_d over Re_D, for the following reasons: (i) since the flow over a Pitot tube is actually an external flow, one would expect that D should be the governing length scale and (ii) Mikhailova and Repik [21] demonstrated the importance of the diameter ratio (β) at low Reynolds numbers ($Re_D < 100$). The importance of the diameter ratio (β) must therefore be evaluated. In order to do so in a quantitative way, all of the data available in the literature were compared with (a) the predictions obtained using the new semi-empirical correlation (i.e. using Re_d as a correlating parameter) and (b) the predictions obtained with Homann's correlation [16] (i.e. using Re_D as a correlating parameter). The root mean square error (RMSE) is used to evaluate the goodness of fit:

$$\mathrm{RMSE} = \left(\frac{\sum_{i=1}^{N_j} \left(Y_{\exp} - Y_{calc}\right)^2}{N_j} \right)^{1/2} \tag{12}$$

where N represents the number of data points in each separate data set 'j', $Y_{\exp}$ is the value of the pressure coefficient (C_p) determined from experimental measurements and Y_{calc} is the C_p value obtained using the specified correlation. Only data sets from the literature where $N_j > 5$ and $Re_D < 100$ were included in the analysis. Table 3 shows the calculated RMSE values, for the two specified correlations, as a function of diameter ratio. Although not shown here, the RMSE values resulting from the use of Mikhailova and Repik's correlation [21] gave similar trends (but different absolute values).

Because it is difficult to obtain an overall sense of the relationship between diameter ratio and goodness of fit (RMSE) – partially because any individual data set for a particular diameter ratio can produce a relatively high RMSE (e.g. both goodness of fit results for $\beta = 0.491$ are relatively poor), because of the scatter (variability) of the measurements themselves, the difference in the root mean square error at each diameter ratio was calculated:

$$\Delta_{RMSE} = \mathrm{RMSE}_{\mathrm{Re}_D} - \mathrm{RMSE}_{\mathrm{Re}_d} \tag{13}$$

The differences are reported, as a function of diameter ratio, in Fig. 7. These results can be interpreted by following the recommendation of Mikhailova and Repik [21]: it is evident that for $\beta \geq 0.6$, the outer tube diameter (and therefore Re_D) should be used as a correlating parameter to determine the pressure coefficient; however, if $\beta < 0.6$, the opening diameter (and therefore Re_d) should be used. To quote Mikhailova and Repik [21]: "The effect of viscosity [on C_p] appears more strongly for tubes with a small value of β than for thin-walled tubes." Based on this logic and the results presented in Fig. 7, however, one could suggest

Table 3
Goodness of fit for pressure coefficient data as a function of β using Re_d or Re_D (for experimental results with $N_j > 5$ and $Re_D < 100$).

	d/D	RMSE Re_d (Eq. (11))	Re_D (Homann)
Sherman (taken from [19])	0.22	0.0536	0.531
Mikhailova and Repik [21]	0.304	0.181	0.448
Present study, PSS	0.32	0.0481	0.450
Present study, PSS	0.37	0.0420	0.127
Mikhailova and Repik [21]	0.491	0.206	0.255
MacMillan [19]	0.60	0.0422	0.0450
Mikhailova and Repik [21]	0.602	0.331	0.137
Mikhailova and Repik [21]	0.695	0.159	0.149
Hurd et al. [23]	0.722	0.0352	0.0610
Mikhailova and Repik [21]	0.739	0.281	0.237
Mikhailova and Repik [21]	0.854	0.244	0.265

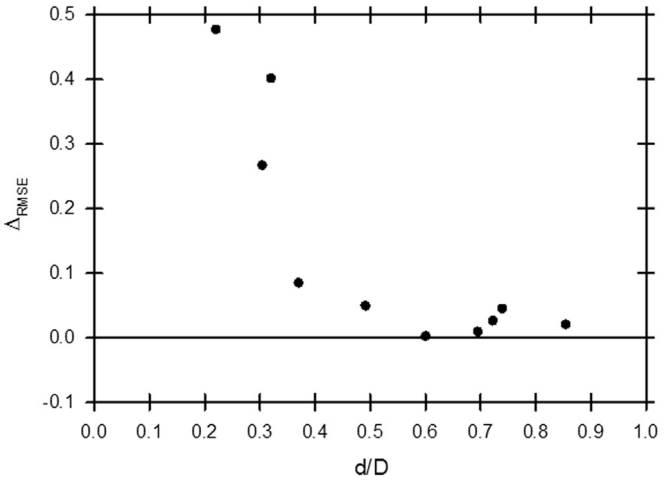

Fig. 7. Difference in the root mean square error (RMSE) between the Homann correlation (based on Re_D) and the new correlation (based on Re_d) as a function of Pitot tube diameter ratio.

that the correlation presented here – which uses Re_d – is clearly superior at $\beta < 0.6$ but provides approximately the same goodness of fit at $\beta \geq 0.6$ as existing correlations based on 'D'.

In summary, the analysis presented here clearly shows that the correlation developed in this study provides a more accurate prediction of the low Reynolds number phenomenon compared to the other correlations identified in the literature, particularly for diameter ratios less than 0.6. In addition to its improved ability to accurately account for the variation of the pressure coefficient (C_p) with Pitot tube Reynolds number (Re_d), the correlation developed in the present study produces physically meaningful values of C_p:

1. It converges asymptotically with Stokes' Law at $\mathrm{Re}_d < 10$, (i.e. $C_p = 6/Re$ when $Re_d < 10$).
2. It reduces to $C_p = 1$ as the Reynolds number is increased beyond the transition Reynolds number, i.e. $Re_t > 35$.

The new correlation proposed here maintains the theoretical aspect of the Barker correction (Eq. (2)) at very low Reynolds number (creeping) flows. It also significantly reduces the offset between Barker's correlation and $C_p = 1$ at the transition Reynolds number, $Re_t = 35$. The low Reynolds number correlation developed in this study applies to hemispherical tipped Pitot tubes with circular openings and Newtonian fluid flow. Based on the results presented here (Fig. 5–7) and the discussion of Mikhailova and Repik [21], the correlation developed in this study is most appropriate for smaller ratios of Pitot tube opening to outside diameter, i.e. $\beta < 0.6$.

In this study hemispherical tipped Pitot tubes were employed, while previous experiments considered blunt tipped or flat-nosed Pitot tubes [13,19,23]. The new correlation, however, provides accurate prediction of the low Reynolds number performance for both the hemispherical tipped Pitot tubes of this study and the flat-nosed Pitot tubes described in the literature. The analysis of the present study suggests that using the Pitot tube opening diameter in calculations is more important than correcting for Pitot tube tip shape, for commonly available industrial Pitot tubes.

6. Conclusions

The conclusions arising from the present study are

1. Because new experimental data were collected for low Reynolds number flows ($10 < Re_d < 100$) with hemispherical tipped

Pitot tubes with low d/D ratios, it was possible to clearly show that local velocities calculated from Pitot tube measurements could not be accurately predicted with Bernoulli's Equation when $Re_d < 35$.

2. A semi-empirical correlation has been developed for hemispherical tipped Pitot tubes, with low d/D ratios, based on the diameter of the Pitot tube opening. Compared to other correlations available in the literature, it more accurately predicts the low Reynolds number effect for the results of this study along with previous results reported in the literature. The correlation reduces to Stokes' Law at very low Reynolds numbers and Bernoulli's Equation at the transition Reynolds number.
3. The correlation developed in this investigation provides a more accurate means to predict Pitot velocities over the entire low Reynolds number range. This includes the intermediate Reynolds number range where inertial effects make Stokes' Law invalid. It also verifies that the opening diameter is the appropriate length scale parameter for hemispherical tipped Pitot tubes with thick walls (i.e. where $d/D < 0.6$).

Acknowledgments

The authors acknowledge the late Dr. C.A. Shook (1934–2006) for his valuable input in the planning and analysis of the results of this study. The financial support of the University of Saskatchewan, NSERC (Natural Sciences and Engineering Research Council of Canada), Saskatchewan Research Council and Syncrude Canada Ltd. is also greatly appreciated. Support of the sponsoring organizations of the *NSERC Industrial Research Chair in Pipeline Transport Processes* (RSS) is gratefully acknowledged.

References

[1] Munson BR, Okiishi TR, Huebsh WW, Rothmayer AP. Fundamentals of Fluid Mechanics. 7th ed.. . Hoboken NJ: John Wiley & Sons, Inc; 2013.
[2] Boetcher SKS, Sparrow EM. Limitations of the standard Bernoulli equation method for evaluating Pitot/impact tube data. Int. J. Heat Mass Transf. 2007;50:782–8.
[3] Vinod V, Chandran T, Padmakumar G, Rajan KK. Calibration of an averaging Pitot tube by numerical simulations. Flow Meas. Instrum. 2012;24:26–8.
[4] Schulenberg T, Stieglitz R. Flow measurement techniques in heavy liquid metals. Nucl. Eng. Des. 2010;240:2077–87.
[5] Banerjee S, Nguyen DM. Mass velocity measurement in steam-water flow by Pitot tubes. AICHE J. 1977;23:385–7.
[6] Davis MR. Response of small Pitot tubes in gas–liquid flows. Int. J. Multiphase Flow 1980;6:369–73.
[7] Hau KF, Banerjee S. Measurement of mass flux in two-phase flow using combination of Pitot tubes and gamma densitometers. AIChE J. 1981;27:177–84.
[8] Hamad FA, He S. Evaluation of hot-film, dual optical and Pitot tube probes for liquid-liquid two-phase flow measurements. Flow Meas. Instrum. 2010;21:302–11.
[9] Mishra R, Singh SN, Seshadri V. Velocity measurement in solid–liquid flows using an impact probe. Flow Meas. Instrum. 1997;8:157–65.
[10] Gillies RG, Hill KB, McKibben MJ, Shook CA. Solids transport by laminar Newtonian flows. Powder Technol. 1999;104:269–77.
[11] Sanders RS, Schaan J, Gillies RG, McKibben MJ, Sun R, Shook CA. Solids transport in laminar, open-channel flow of non-Newtonian slurries. In: Proceedings of the 15th International Conference on Hydrotransport, Banff, Canada BHR Group, Cranfield UK, 3–5 June 2002, pp. 597–611.
[12] Gillies RG, Sun R, Sanders RS, Schaan J. Lowered Expectations: the impact of yield stress on sand transport in laminar, non-Newtonian slurry flows. J. SAIMM 2007;107:351–8.
[13] Barker M. On the use of very small Pitot tubes for measuring wind velocity. Proc. R. Soc. Ser. A 1922;101:435–45.
[14] Schlichting H. Boundary Layer Theory. 7th ed.. New York: McGraw-Hill; 1978.
[15] Folsom RG. Review of the Pitot tube. Trans. ASME 1956;78:1447–60.
[16] Homann F. The effect of high viscosity on the flow around a cylinder and around a sphere, University of California, Berkeley, Inst. of Eng. Res., Report HE-150-88, 16+7p.
[17] Chambre PL. The theory of the impact tube in a viscous compressible gas, In: Inst. Eng. Res., UC Berkeley, Berkeley, Report HE-150-50, 6+5p.
[18] Perry RH, Green DW. Perry's Chemical Engineers' Handbook. 7th ed.. New York: McGraw-Hill; 1997.
[19] MacMillan FA. Viscous effects on Pitot tubes at low speeds. J. R. Aeronaut. Soc. 1954;58:570–2.
[20] MacMillan FA. Viscous effects on flattened Pitot tubes at low speeds. J Roy Aero Soc 1954;58:837–9.
[21] Mikhailova NP, Repik EU. Effect of the viscosity on the readings of total-head tubes with small velocities of the flow. Izvestiya Akademii Nauk SSSR, Mekhanika Zhidkosti i Gaza 1976;1:136–9 (Translated).
[22] Mikhailova NP, Repik EU. Influence of viscosity on the readings of very small flattened Pitot tubes at low flow velocities. Izvestiya Akademii Nauk SSSR, Mekhanika Zhidkosti i Gaza 1979;6:148–52 (Translated).
[23] Hurd CW, Chesky KP, Shapiro AH. Influence of viscous effects on impact tubes. Trans. ASME, J. Appl. Mech. 1953;75:253–6.
[24] Chebbi B, Tavoularis S. Pitot-static tube response at very low Reynolds numbers. Phys. Fluids A 1991;3:481–3.
[25] Spelay RB. Solids transport in laminar open channel flow of non-Newtonian slurries (Ph.D. thesis). Canada: University of Saskatchewan; 2007.
[26] Rhie CM, Chow WL. Numerical study of the turbulent flow past an airfoil with trailing edge separation. AIAA J. 1983;21:1525–35.
[27] Barth TJ, Jesperson DC. The design and application of upwind schemes on unstructured meshes. AIAA 1989:89–0366.
[28] Press WH, Flannery BP, Teukolsky SA, Vetterling WT. Numerical Recipes in C: The Art of Scientific Computing. 2nd ed.. Cambridge UK: Cambridge University Press; 1992.